Interacting force estimation during blade/seal rubs

Romain Mandard, Jean-François Witz, Xavier Boidin, Jacky Fabis, Yannick Desplanques, Jean Meriaux

Tribology International ■ (■■■■) ■■■–■■■

Contents lists available at ScienceDirect

Tribology International

journal homepage: www.elsevier.com/locate/triboint

Interacting force estimation during blade/seal rubs

Romain Mandard [a,b,c,e,*], Jean-François Witz [a,c], Xavier Boidin [a,b,c], Jacky Fabis [d], Yannick Desplanques [a,b,c], Jean Meriaux [e]

[a] Univ Lille Nord de France, F-59000 Lille, France
[b] ECLille, LML, F-59650 Villeneuve d'Ascq, France
[c] CNRS, UMR 8107, F-59650 Villeneuve d'Ascq, France
[d] ONERA, The French Aerospace Lab, F-59000 Lille, France
[e] SNECMA, site de Villaroche, F-77550 Moissy-Cramayel, France

ARTICLE INFO

Article history:
Received 12 September 2013
Received in revised form
12 December 2013
Accepted 16 January 2014

Keywords:
Blade–seal interaction
Abradable material
Force estimation

ABSTRACT

Abradable seals are used in aeronautical compressors to minimize the blade–casing clearance while ensuring the integrity of the mechanical parts in the invent of contact. Considering the tight clearance, in-flight blade–seal interactions may occur and have to be taken into account when designing abradable seals. The blade–seal interacting force is difficult to access but constitutes a key feature to understand the phenomena and to develop numerical models. The present paper aims to present an experimental methodology to estimate the blade–seal interacting force from indirect measurements. The methodology has been applied to a short interaction produced on a dedicated test rig in conditions representative of the full-scale configuration. The obtained force was correlated with the wear profile of the abradable seal.

1. Introduction

The minimization of the blade–casing clearance is a key factor to achieving compressor efficiency in turbojet engines. Minimizing the gap between the rotating blades and the surrounding casing to few tenths of millimeters has been shown to reduce leakage flows and consequently improves efficiency but can also be critical for the engine integrity. During operation, the engine is subjected to differential thermal expansions between the rotor and the stator as well as accelerations arising from aircraft maneuvring and vibrations. The relative rotor–stator displacements induced may lead to zero clearance and critical blade–casing interactions. In compressor stages, the casing is coated with a sacrificial abradable seal. In the event of blade-casing contact, the blade tip abrades the coating, which has been designed to be easily worn. Nevertheless, severe abradable seal wear and blade cracks due to fatigue may occur and have been encountered in full-scale experiments [1].

Understanding and modelling blade–seal contact occurrences require experimental data such as of seal wear, blade dynamics and blade–seal interacting force. It has been shown in full-scale experiments that the wear profile of the abradable coating and the blade dynamics are closely linked. Indeed, Millecamps et al. [2] reported a wave-shaped wear profile of the abradable coating after a blade–casing contact experiment of several minutes. The number of lobes within the circumferential seal wear profile was found to be correlated to the number of blade bending oscillations per revolution. Experimental knowledge of interacting force, seal wear profile and mechanisms are paramount to the implementation of wear laws in industrial codes. Full-scale tests are, by nature, the most representative experiments but are limited in terms of instrumentation because of the complexity of the machine. The force between the blade tip and the abradable coating constitutes a relevant information but is tricky to access. In addition, full-scale experiments are very difficult to analyze on the contact time-scale (few milliseconds).

Different kinds of research test rigs have been developed to study the interactions between blades and abradable coatings, with different levels of in-service representativeness. Sutter et al. [3] and Cuny et al. [4] developed facilities for identifying the interacting force and wear mechanisms pertaining to abradable materials (AlSi-Polyester) for relative speeds of up to 100 m s^{-1} and 270 m s^{-1}, respectively. In these experiments, abradable samples were launched into interaction with a cutting tool made of steel or titanium alloy. Stringer and Marshall [5] and Fois et al. [6] investigated the wear rates, the wear mechanisms and the adhesive transfers between an abradable AlSi-hBN coating and a rotating titanium blade for relative velocities of 100 m s^{-1} to 200 m s^{-1}. The experiments developed by Padova et al. [7] and

* Corresponding author at: Ecole Centrale de Lille, Cité Scientifique, CS20048, F-59651 Villeneuve d'Ascq Cedex, France.
E-mail address: romain.mandard@centraliens-lille.org (R. Mandard).

http://dx.doi.org/10.1016/j.triboint.2014.01.026
0301-679X

at Sulzer-Innotec [8,9] are sufficiently representative of full-scale tangential speeds (up to 400 m s^{-1}) and temperatures in the case of the Sulzer-Innotec experiment. In both experiments, a small blade was rotated to rub against a coated and static sector of casing. Casings were instrumented with piezo-electrical sensors in order to evaluate the blade–casing interacting force. The test rigs presented in [3–9] allow high relative speeds and precise control of incursion depths and speeds. However, in simplified experiments, very little attention has been paid to the analysis of couplings between the dynamics of a flexible blade and the abradable seal wear, which have been reported to be potentially critical for the engines [2].

For the purpose of our study, a test rig was developed to reproduce interactions of short duration between a flexible blade made of titanium (TA6V) and an abradable AlSi-Polyester coating. The configuration has been simplified with respect to the compressor case or the experiment of Padova et al. [10], while being representative of the in-service situation in terms of materials, rotor–stator relative speed and abradable seal temperature. The chosen configuration and the comprehensive instrumentation allow to access the tangential and normal components of the interacting force as well as the wear profile of the abradable seal.

The present paper aims to describe the methodology implemented for the estimation of the blade–seal force, during interactions of a few tens of milliseconds. The experiment – test rig and measurements – is presented in the first section of the paper. The second section is devoted to the methodology for estimating the force, which is based on an analytical description of the incursion cell of the test rig. Results are presented in the third section where the estimated force is correlated with the wear profile of the abradable coating.

2. Blade/seal interaction experiment

2.1. Test rig

In engines, blades have complex geometries and undergo rotary motion. The static casing facing the blades is coated with an abradable seal as shown in Fig. 1a. Therefore, the location of interaction between the blade tip and the abradable coating is rotating. In order to allow instrumentation and analysis of short-duration interactions, the configuration was modified for the test rig (Fig. 1b). The relative blade–seal motion is created by spinning a cylinder, whose external surface is coated with an abradable seal. The interaction is generated by translating the blade toward the rotating seal. In this study, the blade was made from titanium alloy (TA6V) and the tested abradable material was an AlSi-Polyester; these materials are used in low-pressure compressors of turbofans. The blade geometry has been simplified in order to better study the bending dynamics. The natural bending frequencies and dynamic stiffness of the simplified blade have been chosen (by setting the length and cross-section) to be similar to that of compressor blades. Curvature reversal of the abradable seal is the main difference between compressor and test rig configurations. However, the two radii of curvature are on the same order of magnitude (several hundred millimeters), which is twice that of the blade tip thickness (2 mm). On the scale of contact, this curvature reversal is not expected to modify the behavior of the abradable material. However, between the two configurations, differences could lie in the number and length of blade rubs within an incursion of the blade root.

The test rig was constructed at ONERA, The French Aerospace Lab. A first version of this test facility was presented by Baïz et al. in [11]. The incursion cell, which is the main part of the test rig, is shown in Fig. 2a. The TA6V blade is fastened to a small rigid unit. Two bendable legs allow the translation of this small rigid unit along the x-axis. This translation is defined as the apparent incursion D_N and is generated by means of an amplified piezo-electric actuator (APA). The coated cylinder (300 mm diam.) is rotated at the experiment revolution speed Ω by means of a brushless motor (Fig. 2b). The maximum tangential speed V_t at the coating periphery is 95 m s^{-1}. The dynamic properties of the incursion cell allow to translate the small rigid unit (i.e. the blade root) towards the abradable seal, back and forth, with an amplitude of 300 μm, in less than one cylinder revolution at the maximum speed. Thus, the incursion cell is capable of achieving interactions, during which the abradable seal is rubbed by a single pass of the blade, as well as multiple-pass interactions. Considering the blade bending motion encountered during interactions, it should be noted that the displacement of the blade root – or apparent incursion D_N – is not the effective penetration of the blade tip into the abradable coating. In order to reach compressor in-service temperatures up to 300 °C, the coating is heated by means of an induction heating system (Fig. 2b). The coated cylinder has a width of 150 mm, which corresponds to 10

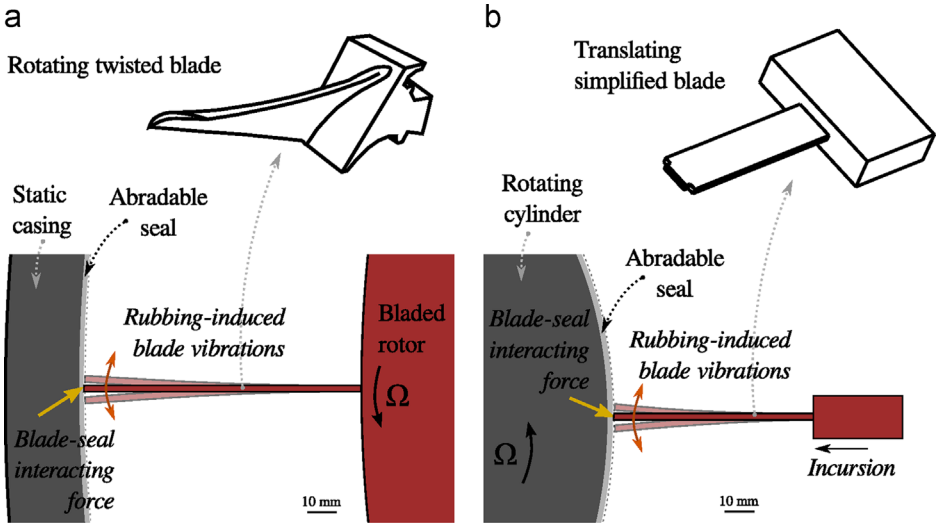

Fig. 1. Schematic representation of blade/seal interaction: (a) actual compressor configuration and (b) reverse test-rig configuration.

Please cite this article as: Mandard R, et al. Interacting force estimation during blade/seal rubs. Tribology International (2014), http://dx.doi.org/10.1016/j.triboint.2014.01.026

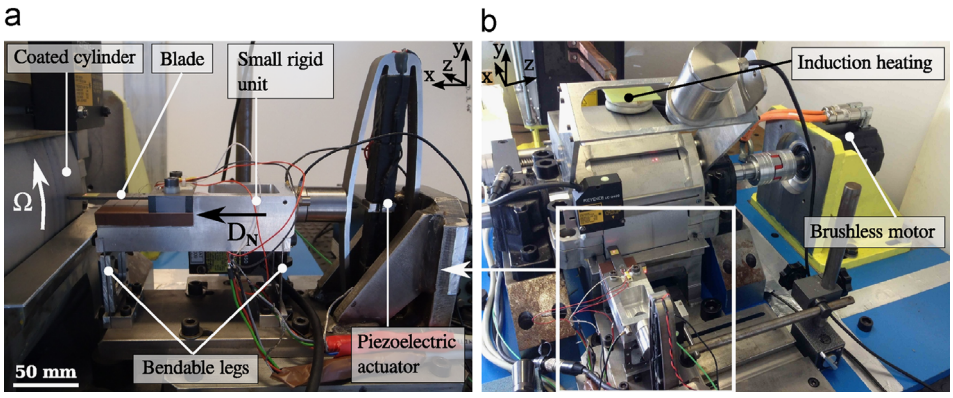

Fig. 2. Test rig operation: (a) incursion cell and (b) overview.

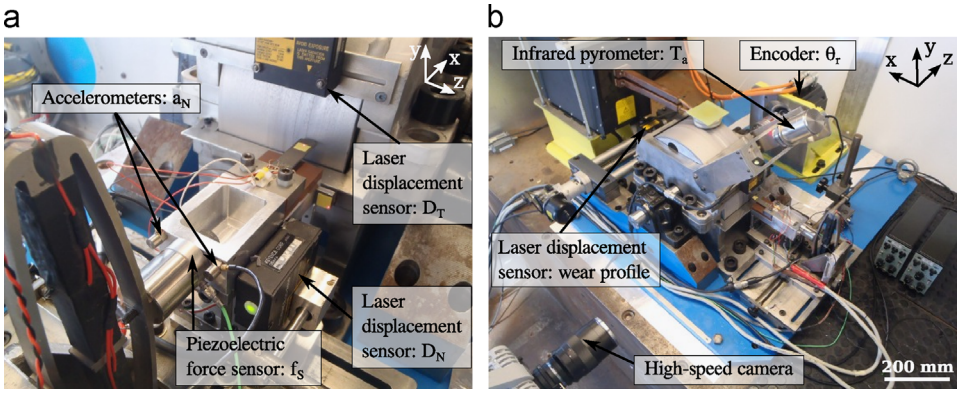

Fig. 3. Test rig instrumentation: (a) incursion cell and (b) overview.

experiment tracks. The incursion cell translates along the *z*-axis to change the experiment track.

As the blade is a very light and flexible structure, the use of a direct force instrumentation at the blade tip is not possible. Therefore, the test instrumentation has been chosen to be representative of blade–seal interactions, to enable the estimation of the interacting force and to be non-intrusive. As shown in Fig. 3a, the apparent incursion D_N is measured via a laser displacement sensor Keyence LC2400. Two others quantities are measured in the normal direction *x*. The acceleration of the small rigid unit a_N is measured by means of two accelerometers B&K 4344 placed on both sides of the incursion axis; a_N is obtained by averaging the two signals. A piezoelectric force sensor Kistler 9031A is used to measure the incursion force f_s. The incursion force f_s and the normal acceleration a_N are used to estimate the normal component of the interacting force. A second laser displacement sensor placed above the blade measures the bending displacement D_T (along *y-axis*). The signal D_T is measured at 17.5 mm from the blade tip and is used to estimate the tangential component of the interacting force.

The blade–seal interaction is captured with a high-speed camera Photron Fastcam SAX at 12 500 frames/s with a resolution of 1024 × 1024 pixels. The scene is lighted up by means of an HMI lamp, in order to catch the blade bending motion as well as the ejection of abradable debris. The wear is quantified with the help of a laser displacement sensor Keyence LKH-082, placed at the rear of the test rig, with an angular offset of 180° from the interaction. The encoder embedded in the brushless motor is used to record the absolute angular position of the rotor θ_r, which enables to readjust the wear profile measurements with the dynamic signals. The surface temperature of the abradable seal T_a is monitored via an infrared pyrometer placed in front of the experiment track.

2.2. Measurement analysis

This section aims to present a typical blade–seal interaction experiment and the measurements used for the force estimation. Prior to the blade–seal interaction, a running-in phase was conducted in order to ensure rubbing over the entire width of the blade tip. Moreover, after running-in, the rubbing surfaces are closer to the compressor in-service conditions. Before running-in, the blade tip was placed tangent to the abradable coating by adjusting the static voltage of the actuator. The running-in was carried out at very low tangential speed (V_t=2 m s^{-1}) and low abradable seal temperature (T_a=50 °C), by increasing gradually and slowly the apparent incursion D_N up to 100 μm (i.e. decreasing the static voltage of the actuator). At the end of the running-in, the blade was moved backward by increasing the static voltage of the actuator in order to set a positive blade–seal clearance before the interaction. Then, the cylinder was rotated at the experiment speed and the abradable seal was heated. During the heating phase, the coated cylinder expands, which supports the blade–seal clearance that was set at the previous step. When the desired temperature was reached (in approx. 30 s), a trigger stopped the heating system and applied the dynamic voltage to the actuator, generating the blade–seal interaction. In this way, the sensors were not affected by the induction heating system during the experiment. The interaction was generated in the following conditions: abradable seal tangential speed V_t of 92 m s^{-1}, abradable seal temperature T_a of 150 °C.

The signals obtained with the different sensors of the incursion cell (Fig. 3a) are presented in Fig. 4. The blade–seal interaction phase corresponds to the time interval [t_i - t_f]. At the start of the interaction, the apparent incursion D_N (red line) was 130 μm, which corresponds to the initial blade–seal clearance (at T_a=150 °C). The maximum value of D_N is 200 μm. Therefore, the

Please cite this article as: Mandard R, et al. Interacting force estimation during blade/seal rubs. Tribology International (2014), http://dx.doi.org/10.1016/j.triboint.2014.01.026

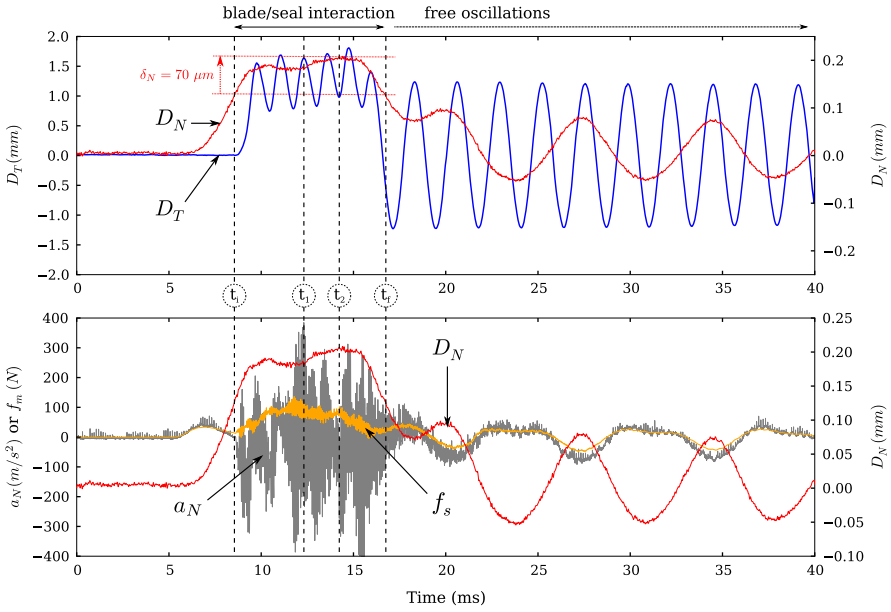

Fig. 4. Raw signals obtained in the experiment: apparent incursion D_N, normal acceleration a_N, incursion force f_s, blade bending displacement D_T. Test conditions: abradable seal tangential speed V_t=92 m s^{-1}, abradable seal temperature T_a = 150 °C. (For interpretation of the references to color in this figure caption, the reader is referred to the web version of this paper.)

effective displacement of the blade foot toward the abradable seal, during the interaction, was δ_N=70 μm. In the tangential direction, the observation of the blade bending displacement D_T (blue line) suggests that a series of blade rubs or impacts occurred during the interaction. High-speed video frames corresponding to times t_i (first contact), t_1 (local maximum for D_T) and t_2 (local minimum for D_T) are shown in Fig. 5. Both the blade bending motion and the ejection of abradable seal debris are visible. The phase following the blade–seal interaction (Fig. 4, after t_f) corresponds to the free oscillations of the incursion cell.

The acceleration a_N (grey line) and the incursion force f_s (orange line) are superimposed in the lower frame in Fig. 4. Several remarks should be made regarding these quantities. Firstly, the incursion force f_s is non-zero and in-phase with the acceleration a_N, before and after the interaction, which indicates that this signal includes an acceleration component. The force f_s itself cannot be considered to be the normal interacting force component and must be compensated, i.e. the accelerometric force must be removed from the signal. Secondly, blade impacts are suggested by the blade bending displacement D_T, while this is not the case in signals f_s and a_N. Higher frequencies than blade-seal rubs are contained in signals f_s and a_N, which means that the interacting force must be estimated over the minimal frequency band allowing the identification of the rubs series.

The data shown in Fig. 4 provide a first and qualitative interpretation of the blade–seal interaction. It should be reminded that the final objective of this study is the estimation of the blade–seal interacting force. The measured quantities and the corresponding sensors have been chosen for this purpose. The methodology for estimating the force is presented in the following section.

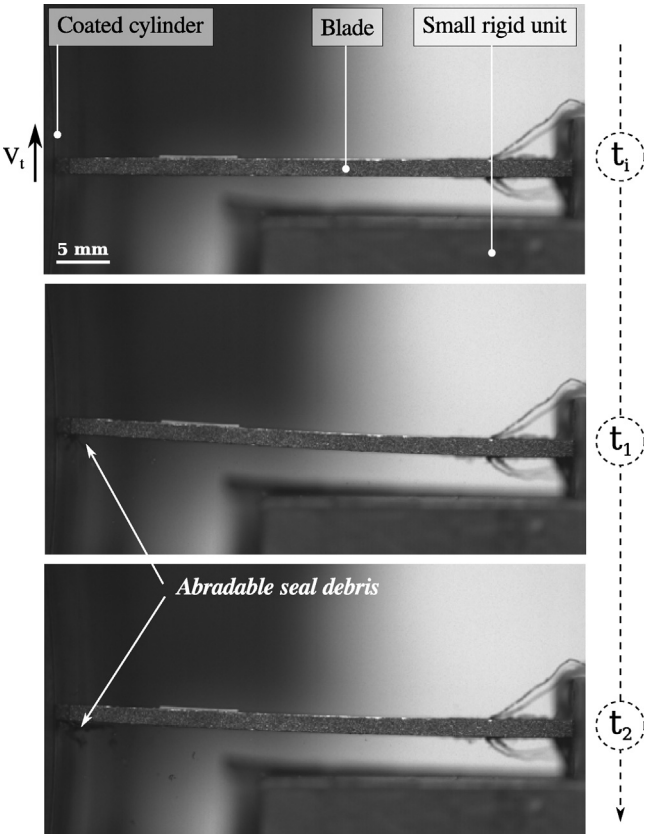

Fig. 5. High-speed imaging of the experiment at t_i, t_1 and t_2.

3. Methodology for estimating the interacting force

Whether in full-scale conditions or in simplified experiments, the normal and tangential force components at the blade tip are difficult to measure because of the nature of the blade, which is a light and flexible structure. The test rig was designed to simplify the blade–seal configuration and the instrumentation, with respect to the compressor configuration. This section aims to estimate the tangential and the normal force components based on the measurements previously presented.

3.1. Analytical model of the incursion cell

Based on the simple design of the incursion cell (CAD view in Fig. 6a), an analytical model is proposed in Fig. 6b. The blade is

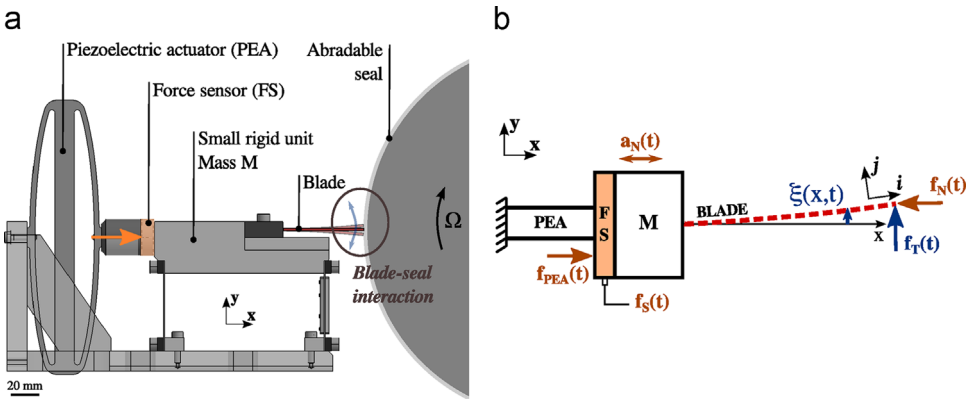

Fig. 6. (a) CAD view and (b) analytical model of the incursion cell.

modelled as a continuous Euler–Bernoulli beam, considering only bending. The compressive displacement of the blade is neglected since the first compression mode of the blade is higher than 10 kHz. The blade bending motion is described by the displacement ξ, function of the blade abscissa x and time t. The bending displacement D_T that was measured is related to ξ as follows: $D_T(t)=\xi(x_f,t)$, where x_f is the location of the laser displacement sensor. The small rigid unit, on which the blade is fastened, is considered as a non-deformable and moving mass M. The motion of the mass M is limited to the normal direction x and its position is described by the apparent incursion $D_N(t)$. Previously, an experimental modal analysis of the incursion cell was carried out, showing that the natural translation modes of the mass M along x-axis (150 and 280 Hz) are lower than the first natural translation mode along y-axis (1400 Hz). This supports that the motion of the mass M along y-axis and the compressive displacement of the blade are not considered. The acceleration $a_N(t)$ is defined as $a_N(t)=\partial^2 D_N(t)/\partial t^2$. The piezoelectric actuator (*PEA*) is modelled as an electromechanical element, supplied with a voltage $V_e(t)$ and delivering a force $f_{PEA}(t)$, along x-axis, to generate the incursion. The piezoelectric force sensor (*FS*), placed between the *PEA* and the mass M, outputs the signal f_s, whose components are detailed in the following.

Regarding the interaction between the blade tip and the abradable seal, the model is based on the assumption that the blade tip is in a free kinematic boundary condition. The interaction is represented by two external forces applied at the blade tip: the normal force $f_N(t)$ and the tangential force $f_T(t)$. This choice has been justified by a previous time-frequency analysis of interaction data. In this analysis, the excited vibrational modes of blades were identified as the first clamped-free bending modes, suggesting a slight influence of the contact stiffness on the blade-seal interaction, in the considered experiments. f_T and f_N are the force components to be estimated. In the Euler–Bernoulli beam model, the rotation of the sections within the beam is assumed to be small. Consequently, the local coordinate system (i, j) of the beam coincides with the global coordinate system (x, y). According to the proposed model (Fig. 6b), the tangential force $f_T(t)$ is associated only to the blade bending motion. Similarly, the normal force $f_N(t)$ influences only the motion of the mass M. Therefore, the two force components can be separately estimated.

3.2. Estimation of tangential force component

According to the previous observations made on the measurements (Fig. 4) and the assumptions associated to the analytical model (Fig. 6), the tangential force f_T acts only on bending of the blade. Therefore, the dynamics of the mass M is not accounted and only the dynamic equations describing the blade are used in this section.

3.2.1. Dynamic equations

The position x_f for the measurement of the bending displacement $D_T(t)=\xi(x_f,t)$ was chosen to be close to the vibration node of the second natural mode of the blade: $x_f/L=0.72$, where L is the blade length. Thus, a very small influence of the higher order modes in the measured displacement D_T is assumed. The blade bending motion around the position x_f is considered as the vibration of the first natural mode:

$$\xi(x,t)=Z_1(x)T_1(t) \tag{1}$$

where $Z_1(x)$ is the first blade natural shape according to the Euler–Bernoulli beam model in the chosen boundary conditions, x is the blade abscissa and $T_1(t)$ is the modal amplitude function of time t. The Lagrange's equations have been derivated to give the dynamic equation:

$$M_1\ddot{T}_1(t)+C_1\dot{T}_1(t)+K_1T_1(t)=F_1(t) \tag{2}$$

where M_1 and K_1 are the modal mass and stiffness of the first natural bending mode, respectively, defined as follows (resp. Eqs. (3) and (4)):

$$M_1=m\int_0^L Z_1(x)^2\,\mathrm{dx} \tag{3}$$

$$K_1=\mathrm{EI}\int_0^L Z_1''(x)^2\,\mathrm{dx} \tag{4}$$

$\dot{T}_1(t)$ is the temporal derivative of $T_1(t)$, $\ddot{T}_1(t)$ is the second temporal derivative of $T_1(t)$, $Z_1''(x)$ is the second spatial derivative of $Z_1(x)$, m is the mass per unit length of the blade, E is the Young modulus of TA6V and I is the moment of inertia of the blade.

Regarding the modal damping C_1, it is defined as a Rayleigh damping and can be expressed as:

$$C_1=4\pi\mu_1 f_1 M_1 \tag{5}$$

where f_1 is the first bending natural frequency. The damping factor μ_1 was identified using the decrease of free oscillations [12]. The modal characteristics calculated for the blade, M_1, K_1, C_1 and f_1, are given in Table 1.

Finally, F_1 is the generalized force:

$$F_1(t)=f_T(t)Z_1(L) \tag{6}$$

where $f_T(t)$ is the tangential force to be estimated; $Z_1(L)$ is the value of the first natural shape at the blade tip that is the point of force application (L is the length of the blade). In order to evaluate $f_T(t)$, we must invert the dynamic linear equation (2).

Please cite this article as: Mandard R, et al. Interacting force estimation during blade/seal rubs. Tribology International (2014), http://dx.doi.org/10.1016/j.triboint.2014.01.026

Table 1
Theoretical modal characteristics of the blade (Euler-Bernoulli beam model).

Mass M_1 (g)	15.3
Stiffness K_1 (N mm^{-1})	106
Damping C_1 (g s^{-1})	90
1st natural frequency f_1 (Hz)	419

3.2.2. Inversion method

The inversion methods of linear systems, for the purpose of force estimation, can be separated into two main groups: the deconvolution methods and the methods based on mechanical models. The principle of deconvolution methods is based on the identification of a transfer matrix that relates the measured quantities and the forces to be estimated [13]. These methods are in general implemented in the frequency domain and are adaptated to complex structures whose analytical description is difficult to obtain. The transfer matrix can be identified either experimentally through modal analysis techniques, or numerically using finite-elements modelling. This kind of method was used in the field of abradable seal rubbing characterization by Cuny et al. [4] and Padova et al. [7].

In our case, the description of the structure motion is reduced to a simple one-degree-of-freedom model and the chosen inversion method uses the analytical equation (2). This method, based on the Kalman filter [14], was published by Ma et al. [15] for the estimation of forces applied on beam structures. The Kalman formalism requires to express the problem as a state space system:

$$\begin{bmatrix} \dot{T}_1(t) \\ \ddot{T}_1(t) \end{bmatrix} = \begin{bmatrix} 0 & I \\ -M_1^{-1}K_1 & -M_1^{-1}C_1 \end{bmatrix} \begin{bmatrix} T_1(t) \\ \dot{T}_1(t) \end{bmatrix} + \begin{bmatrix} 0 \\ M_1^{-1} \end{bmatrix} F_1(t) \tag{7}$$

$$D_T(t) = \underbrace{[Z_1(x_f)\ \ 0]}_{H} \begin{bmatrix} T_1(t) \\ \dot{T}_1(t) \end{bmatrix}. \tag{8}$$

Eq. (7) is Eq. (2), rewritten as a first order equation, with $X = [T_1\ \dot{T}_1]^T$. Eq. (8) is the observation equation, where the matrix H relates the degree of freedom T_1 (modal amplitude of the first bending natural mode) to the observed quantity D_T (blade bending displacement measured with the laser displacement sensor). Then, the state space system must be time-discretized: $t = kT$, where k is the discretization index and T is the chosen discretization period. The algorithm proposed by Ma et al. [15], at a time step k, works in two stages. Firstly, an estimation $\overline{X}(k)$ of the system state for an unknown force is calculated with the equations of the Kalman filter. The following quantities related to the Kalman filter are also calculated: the innovation $\overline{Z}(k)$, the innovation covariance $S(k)$ and the Kalman gain $K_a(k)$. Secondly, a quadratic form, function of the innovation $\overline{Z}(k)$ and the unknown force $F(k)$, is minimized by means of a recursive least-square algorithm, yielding the estimated force $\tilde{F}(k)$. The inversion method has been summarized in Fig. 7, in the form of a diagram. The algorithm, available in Ma's paper [15], was implemented in Python language for our study. It should be noted that in the Kalman algorithm, two parameters must be set: the process and measurement noises [14], which are assumed to be independent white noises. In our application the process noise covariance was set to $1N^2$. The measurement noise covariance was set to 2.5×10^{-13} m^2, which corresponds experimentally to the uncertainty of the laser displacement sensor that measured D_T.

3.3. Estimation of normal force component

Several strategies were studied in order to estimate the normal force. A similar approach to that used for the estimation of the tangential force was first considered: a dynamic electromechanical equation of the incursion cell in the normal direction, combined with the measurement of the degrees of freedom and the implementation of the inverse method used previously. The considered model was based on the work published by Rodriguez-Fortun et al. [16]. It included the dynamic and electromechanical properties of the piezoelectric actuator and the moving mass M. This model was relevant for simulating unladen incursion, i.e. incursions without blade–seal contact. However, there were two limitations for the implementation of the inverse method. Firstly, the modal analysis of the APA-type piezoelectric actuator indicated the presence of two natural vibration modes [17], which were not represented in the electromechanical model since the piezoelectric actuator was modelled with a single stiffness. Depending on the external force during the blade–seal interaction, the second vibration mode could be excited and the model was wrong in this case. Secondly, piezoelectric actuators are subjected to hysteresis, which can be modelled, for example, with a Bouc–Wen model [18]. Such an electromechanical model is not linear and the method of inversion could not be applied.

Consequently, the employed strategy allow to work around the two abovementioned issues. Rather than the inversion of a dynamic equation with kinematic data as input, the quantities measured in the normal direction x (Fig. 6) enable the estimation of the normal force component via an accelerometric compensation equation. Different techniques for accelerometric compensation of force sensors can be found in the literature. Tounsi and Otho [19] proposed a method for the compensation of a three-dimensional force sensor in the frequency domain for an application in the field of machining. In our case, the problem is simplified to one dimension and the compensation can be processed in the time domain, as done by Guegan et al. [20] for an experimental arrangement with Hopkinson bars.

3.3.1. Accelerometric compensation equations

As assumed in Section 3.1, the compressive displacement of the blade is neglected. Under this assumption, the forces acting on the force sensor are: the force delivered by the actuator, f_{PEA}, and the normal component of the interacting force, f_N. Moreover, it has been shown in Section 2.2 that an accelerometric component is contained in the output signal of the force sensor f_s. Thus, the signal f_s can be written as:

$$f_s(t) = f_N(t) + f_{PEA}(t) + Ma_N(t) \tag{9}$$

where M is the moving mass representing the small rigid unit (Fig. 6). The force f_{PEA} is indirectly measured through the simple electromechanical relation that follows [21]:

$$f_{PEA}(t) = b_{em}V_e(t) \tag{10}$$

where V_e is the dynamic voltage applied to the actuator, which was acquired during the experiment, and b_{em} is an electromechanical factor. In order to access the force f_N through Eqs. (9), (10) and the measurements f_s, a_N and V_e, the parameters M and b_{em} must be identified.

3.3.2. Identification of the parameters

The parameters were identified in two steps, starting with the mass M. During free oscillations of the incursion cell, Eq. (9) becomes:

$$f_s(t) = Ma_N(t) \tag{11}$$

The free oscillations were generated with an impact hammer. The recorded signals f_s and a_N are presented in Fig. 8a. Note that both signals are a composition of the two natural modes identified at 150 and 280 Hz (cf. Section 3.1), induced by the design of the actuator (cf. introduction of Section 3.3). The mass

Please cite this article as: Mandard R, et al. Interacting force estimation during blade/seal rubs. Tribology International (2014), http://dx.doi.org/10.1016/j.triboint.2014.01.026

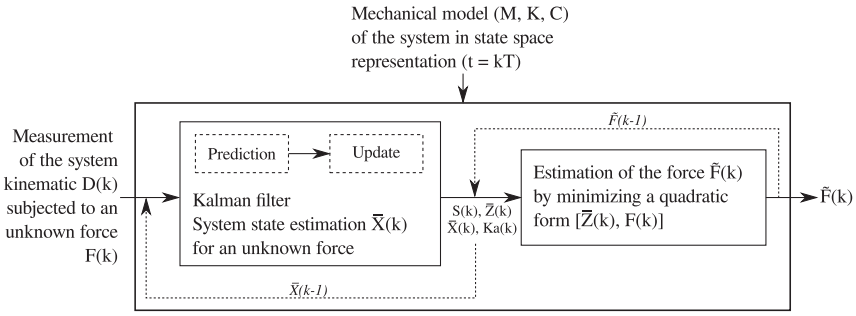

Fig. 7. Diagram of the inversion method proposed by Ma et al. [15].

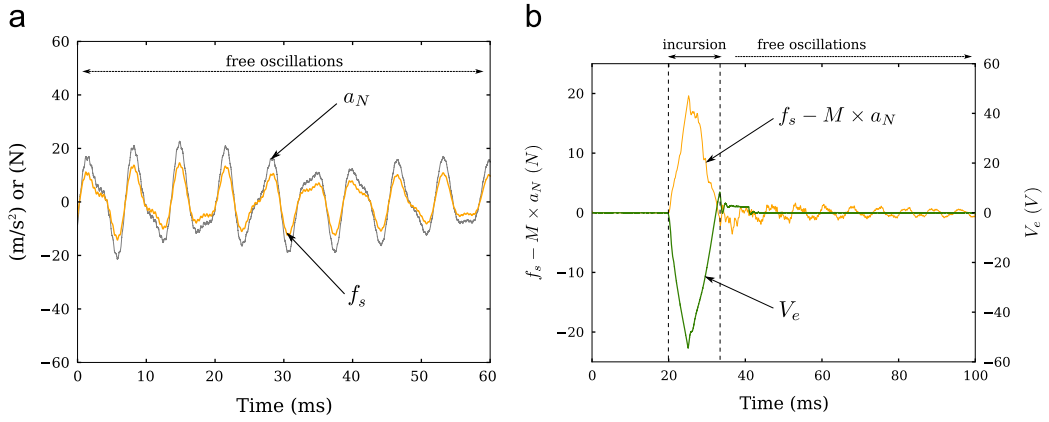

Fig. 8. Experimental data used for the identification of the parameters M and b_{em}: (a) free oscillations of the incursion cell and (b) unladen incursion.

M was researched as the value minimizing the quantity $E_M = (1/N)\sum_{i=0}^{N}[f_s(i) - Ma_N(i)]^2$ where N is the number of points in the signals. The identified value is $M = 0.63$ kg.

In order to identify the electromechanical coefficient b_{em}, an unladen incursion was produced, i.e. the incursion cell was excited with a dynamic voltage, without blade–seal interaction ($f_N(t) = 0$). In this configuration, Eq. (9) becomes:

$$f_s(t) - Ma_N(t) = b_{em}V_e(t) \tag{12}$$

The measured quantities $f_s - Ma_N$ and V_e are shown in Fig. 8b. The profiles of the curves indicate that the simple electromechanical equation (10) is valid. The coefficient b_{em} was researched as the value minimizing the quantity $E_{b_{em}} = (1/N)\sum_{i=0}^{N}[f_s(i) - Ma_N(i) - b_{em}V_e(i)]^2$ where N is the number of points in the signals. The identified value is $b_{em} = -0.36$ N/V.

Finally, the normal force f_N can be estimated by combining Eqs. (9) and (10), and the parameters M and b_{em}:

$$f_N(t) = f_s(t) - Ma_N(t) - b_{em}V_e(t) \tag{13}$$

where f_s, a_N and V_e were measured during the experiment.

As mentioned in Section 2.2, it is necessary to filter the signals f_s and a_N, since the corresponding sensors are sensitive to frequencies higher than the blade–seal rubs frequency (≈ 1 kHz). Thus, the signals f_s and a_N measured during blade–seal rubbing were low-pass filtered using a filtering window with a constant gain ($=1$) over the $[0, f_c]$ frequency band and an exponential decrease of the gain for $f > f_c$, where f_c is the chosen cut-off frequency. The smooth decrease of the gain limits the introduction of parasitic oscillations, known as the Gibbs effect. In our study, the cut-off frequency was set at 2.5 kHz. This ensures to preserve the dynamics of the blade–seal rubs while removing the high-frequency content that complicates the interpretation of the experiment. The low-pass filter was validated by simulating a normal impact at the blade tip with a modal hammer. The impact force applied with the hammer was representative of a blade–seal impact in terms of duration and force amplitude. It was verified that no loss of magnitude nor phase shift occurred when filtering the force signal recorded by the hammer.

4. Results

4.1. Blade/seal interacting force

The two components of the interacting force were estimated according to the methods detailed in Sections 3.2 and 3.3, for the tangential and normal components, respectively. The dimensionless forces are shown in Fig. 9 (bottom frame). The two forces, computed from independent measurements and methods, are in-phase and in the form of a series of 7 rubs. After the interaction (i.e. during the free oscillations) the forces should be theoretically equal to zero. The small oscillations in the forces correspond to the noise of the complete estimation process, which is less than 10% of the maximum values. Several remarks can be made about the results. Firstly, it should be noted that the 7th rub is difficult to detect by observing only the bending displacement D_T. Indeed, the last contact occurred during the backward movement of the blade in the normal direction , which modified the nature of the rub (no bounce). This indicates that observing the displacements is not sufficient to analyze the blade–seal rubbing accurately. The introduction of dynamic modelling (as done for the tangential force) or the measurement of dynamic quantities (as done for the normal force) are required for a proper analysis. Secondly, the maximum values for f_T and f_N are not obtained at the same time during the experiment. The maximum normal force f_N^{max} is reached at the first rub, when the initial bending displacement and speed are zero.

Please cite this article as: Mandard R, et al. Interacting force estimation during blade/seal rubs. Tribology International (2014), http://dx.doi.org/10.1016/j.triboint.2014.01.026

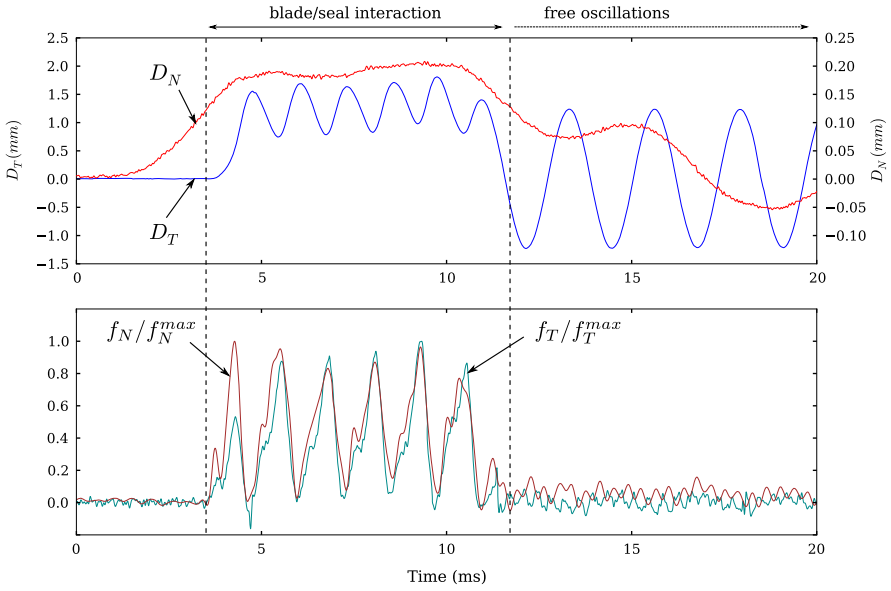

Fig. 9. Normalized components of the interacting force. Test conditions: tangential speed $V_t = 92$ m s^{-1}, abradable seal temperature $T_a = 150$°C.

The maximum tangential force f_T^{max} is obtained at the fifth rub, when the bending displacement D_T is decreasing after the fourth bounce. This clearly shows the complex nature of the blade–seal tribological system. The friction factor f_T/f_N varies during the interaction depending on the blade–seal relative motion (amongst others). The friction factor at the first rub reaches $f_T/f_N = 0.2$ while reaching $f_T/f_N = 0.6$ at the fifth rub. Considering these variations, the use of a constant friction coefficient in the description of the blade–seal interaction may be inappropriate, especially for numerical simulation purpose.

It is worth nothing that the multiple rubs within the interaction are the result of the blade dynamics properties. The latter were chosen to be close to the full-scale condition. The seven rubs have a characteristic time of 1 ms, corresponding to a rub length on the order of 100 mm. In the paper by Padova et al. [7], blade-casing interactions led to five or six rubs, on the order of 0.5 ms within a 90 μm incursion of the casing towards the spinning blade tip. Rub lengths were not explicitly reported in the paper but can be estimated around 170 mm, considering rotational and tangential speeds. The full-scale blade–casing interactions reported in the paper by Millecamps et al. [2] led to a 6 or 7-lobe wear shape of the abradable seal. The blade bending vibration was found to be in phase with the wear lobes. This indicates the occurrence of six or seven 20° rubs per revolution. Under the assumption of a 500 mm radius compressor, we can estimate the rub length about 180 mm. Therefore, the rubs obtained in the present experiment, in the reversed configuration, are representative of the standard blade–casing configuration in terms of length and duration. However, the main difference lies in the analysis of wear. In the study by Padova et al. [7], the multiple rubs occurred on the same sector of casing, once per revolution.In the study by Millecamps et al. [2], the multiple rubs per revolution were distributed over the whole circumference of the casing but the experiment was stopped after a very large number of revolutions. The rubs obtained in the present experiment are the result of a single pass of the blade, which gives a complementary approach for the wear analysis of the abradable coating.

4.2. Abradable seal wear

The seal wear and the corresponding interacting force are paramount to the study of abradable seals. During engine operation, the abradable material must wear with minimum rubbing-induced forces, in order to protect the blades. Concurrently, large wear rates increase the blade–casing clearance, which is detrimental for the engine performance. The design of abradable materials and the prediction of their lifetimes require to experimentally investigate the relation between force and seal wear, under different operating conditions (blade–seal tangential speed V_t, abradable temperature T_a). The test rig was designed to allow wear profile measurements as well as post-mortem analysis in order to identify the wear mechanisms. This section aims to correlate the abradable wear profile with the estimated force but does not intend to highlight wear mechanisms. However, it should be noted that, parallel with this work, SEM observations and X-Ray tomographic scans of the rubbed material (running-in only and running-in followed by the interaction) were carried out to investigate the wear mechanisms. In particular, preliminary analysis showed that the initial thermal-sprayed and machined material was successively and gradually affected by the running-in phase (cf. Section 2.2) and then the interaction. The first investigations pointed out a combination of several wear mechanisms: shear associated to the formation and ejection of debris (Fig. 4), grooving and densification. Such wear mechanisms, in the case of aluminium-based abradable materials, were observed on in-service seals [22] and in laboratory experiments [6,8]. It should be reminded that the blade–seal interaction detailed in this paper is a blade single-pass experiment since the interaction was conducted over less than one cylinder revolution. The characterization of wear is usually performed after few [10] or many [6] blade rubs, which is more representative of the in-service situation. However, the present experiment provides a complementary approach to that, with the aim of measuring abradable wear profiles of single-pass rubs. In the full-scale experiments by Millecamps et al. [2] and Batailly et al. [1], wear measurements were conducted after several minutes of blade–seal rubbing. Therefore, the abradable seal wear per revolution - useful for numerical simulation purposes - could not be considered.

4.2.1. Wear profile measurement

The measurement technique for the abradable wear profile, introduced in Section 2.2, is detailed in the present section. A laser displacement sensor is placed at the rear of the test rig with a 180°

Please cite this article as: Mandard R, et al. Interacting force estimation during blade/seal rubs. Tribology International (2014), http://dx.doi.org/10.1016/j.triboint.2014.01.026

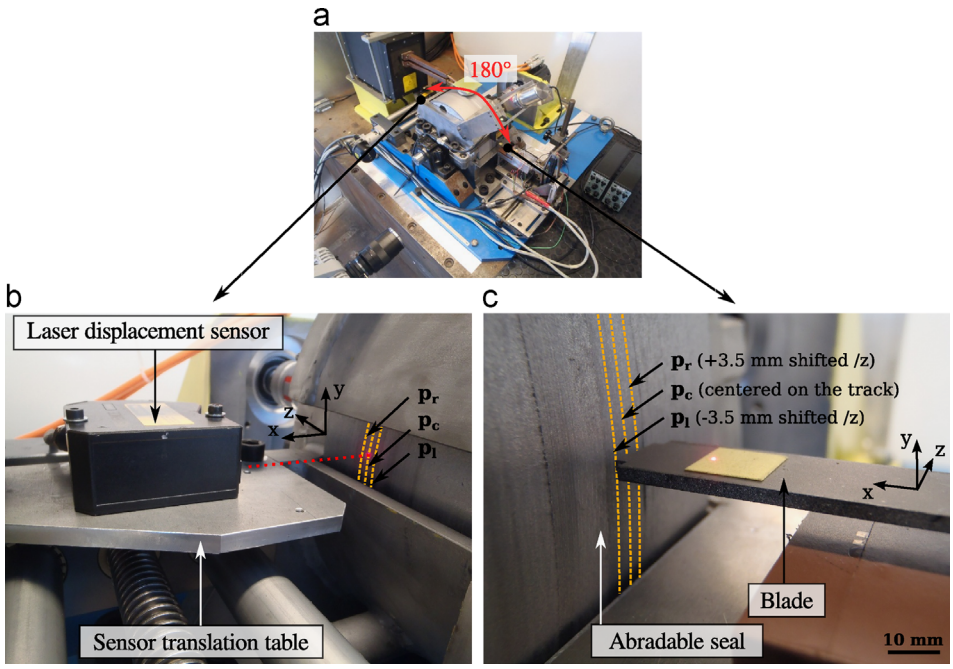

Fig. 10. Wear profile measurement of the abradable track: (a) test rig overview, (b) measurement with the laser displacement sensor at the rear of the test rig, and (c) locations of the 3 measurements in front of the blade tip.

angular offset from the interaction, as shown in Fig. 10a. The sensor is fixed on a table allowing the translation along the z-axis in order to position the sensor in front of the experiment track (Fig. 10b). For one experiment, three profiles, namely p_c, p_l and p_r are measured in the center, on the left side and on the right side of the experiment track, respectively (Fig. 10c).

The track profiles are measured after the running-in phase (i.e. before the blade–seal interaction) and after interaction, at a very low revolution speed of the cylinder $\Omega=1$ tr/min. The laser spot of the displacement sensor has a diameter of 70 μm. Consequently, the measurement is sensitive to the porosity of the abradable material, which can be locally deeper than the wear depth of a blade–seal impact. Furthermore, the wear length induced by a blade impact is on the order of several tens of millimeters. The profile measurements were low-pass filtered to be interpreted on the rub scale. The spatial cut-off frequency f_c^S was chosen to be equivalent to the time cut-off frequency used for filtering the normal force ($f_c=2.5$ kHz), at low tangential speed $V_t=20$ m/s. The spatial cut-off frequency is calculated from the relation:

$$f_c^S = \frac{f_c}{V_t} \tag{14}$$

4.2.2. Correlation with the interacting force

Using the absolute angular position θ_r provided by the encoder of the motor, the profile measurements can be readjusted with the force components. The initial and final profiles p_c, p_l and p_r are shown in Fig. 11, as well as the normalized force components. The curves are plotted as functions of time and cylinder angular position θ_r. Wear corresponds to a positive difference between the final and the initial profiles. Before analyzing these data, it should be precised that the displacement sensor was repositioned after the experiment, for the profiles p_l and p_r (left and right sides of the track, respectively). Therefore, considering the uncertainty in repositioning, the final profile may be slightly shifted from the initial one along z-axis (Fig. 10). Regarding the profile p_c in the center, the sensor was hold at the same location for the initial and final measurements. Work is on-going to address this issue. Firstly, despite therunning-in phase, the three wear profile measurements show that wear depths are slightly higher on the left side of the experiment track. Secondly, the three wear profiles are in-phase with the forces, which indicates that the dynamic measurements, the methods used to estimate the forces and the quasi-static profilometry are consistent. Moreover, the maximum wear depth is on the order of 35 μm, which is lower than the effective apparent incursion of the blade ($\delta_N=70$ μm, cf. Fig. 4). These results clearly underline the influence of blade dynamics on blade-to-seal rubbing.

5. Conclusions

During blade–seal interactions, rubbing between the blade tip and the abradable seal is coupled with blade dynamics. In order to study these couplings, a specific test rig has been developed and is capable of generating very short blade–seal interactions under representative incursion conditions of full-scale operation. The simplified configuration has allowed a large instrumentation of the experiment in order to estimate the interacting force. Both the measurements and the methodology for the force estimation have been presented in this paper. The tangential component was estimated using the measurement of the blade bending motion, a simple analytical model of the blade and a technique of model inversion. The normal component was estimated through force and acceleration measurements, combined in an accelerometric compensation equation. The methodology was applied to an experiment conducted with a TA6V blade and an abradable AlSi-Polyester coating. The two force components obtained were in-phase, in the form of a series of short rubs. The wear profile of the abradable coating was also measured, showing wear lobes in-phase with the estimated force.

Acknowledgments

This study was supported by SNECMA and received the financial support of the French Ministry of Higher Education and Research, both of whom are gratefully acknowledged. Thanks are

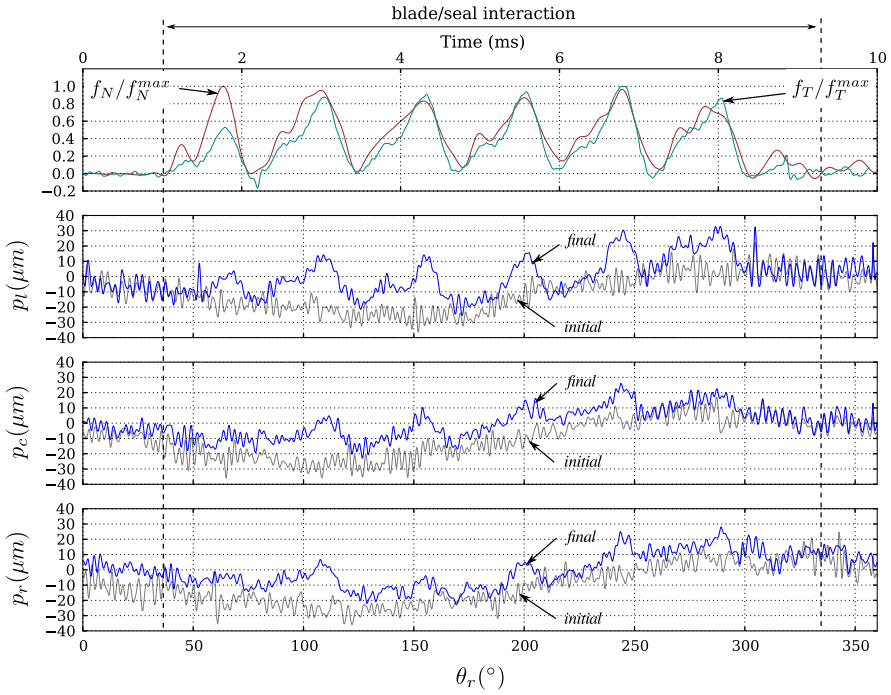

Fig. 11. Initial (grey lines) and final (blue lines) profiles of the abradable track (p_l: left-side profile, p_c: centered profile, p_r: right-side profile) and normalized force components vs angular position θ_r. Wear is positive. (For interpretation of the references to color in this figure caption, the reader is referred to the web version of this paper.)

also due to the International Campus on Safety and Intermodality in Transportation (CISIT), the Nord-Pas-de-Calais Region, the European Community, the Regional Delegation for Research and Technology, the Ministry of Higher Education and Research, and the National Centre for Scientific Research. The authors thank François Lesaffre (*ECLille, LML*) for his technical and continued contribution to the study.

References

[1] Batailly A, Legrand M, Millecamps A, Garcin F. Numerical–experimental comparison in the simulation of rotor/stator interaction through blade-tip/abradable coating contact. J Eng Gas Turbines Power-Trans. ASME 2012;134.
[2] Millecamps A, Brunel J-F, Dufrenoy P, Garcin F, Nucci M. Influence of thermal effects during blade–casing contacts experiments. In: Proceedings of the ASME IDETC/CIE, USA; 2009.
[3] Sutter G, Philippon S, Garcin F. Dynamic analysis of the interaction between an abradable material and a titanium alloy. Wear 2006;261:686–92.
[4] Cuny M, Philippon S, Chevrier P, Garcin F. Etude expérimentale des interactions dynamiques aube/carter. In: Proceedings of 20e Congrès Français de Mécanique, France; 2011 (in French).
[5] Stringer J, Marshall MB. High speed wear testing of an abradable coating. Wear 2012;294–295:257–63.
[6] Fois N, Stringer J, Marshall MB. Adhesive transfer in aero-engine abradable linings contact. Wear 2013;304:202–10.
[7] Padova C, Barton J, Dunn MG, Young G, Adams Ma, Adams Mi. Development of an experimental capability to produce controlled blade tip/shroud rubs at engine speed. J Turbomach Trans ASME 2005;127.
[8] Schmid RK. New high temperature abradables for gas turbines [Ph.D. thesis]. Zurich, Swiss: Swiss Federal Institute of Technology; 1997.
[9] Bounazef M, Guessasma S, Ait Saadi B. The wear, deterioration and transformation phenomena of abradable coating BN-SiAl-bounding organic element, caused by the friction between the blades and the turbine casing. Mater Lett 2004;58:3375–80.
[10] Padova C, Barton J, Dunn MG, Manwaring S. Experimental results from controlled blade tip/shroud rubs at engine speed. J Turbomach Trans ASME 2007;129.
[11] Baïz S, Fabis J, Boidin X, Desplanques Y. Experimental investigation of the blade/seal interaction. Proc Inst Mech Eng Part J J Eng Tribol 2013;227(9):980–995.
[12] Clough RW, Penzien J. Dynamics of structures. McGraw-Hill, NY, USA; 1975.
[13] Inoue H, Harrigan JJ, Reid SR. Review of inverse analysis for indirect measurement of impact force. Appl Mech Rev 2001;54.
[14] Welch G, Bishop G. An introduction to the Kalman filter. From UNC-Chapel Hill, TR95-041; 2000, ⟨http://www.cs.unc.edu⟩.
[15] Ma C-K, Chang J-M, Lin D-C. Input forces estimation of beam structures by an inverse method. J Sound Vib 2003;259(2):387–407.
[16] Rodriguez-Fortun JM, Orus J, Alfonso J, Gimeno FB, Castellanos JA. Flatness-based active vibration control for piezoelectric actuators. IEEE/ASME Trans Mechatron 2013;18.
[17] Olympio RK, Poulin-Vittrant G. A honeycomb-based piezoelectric actuator for a flapping wing MAV. Proc SPIE 2011;7977.
[18] Ismail M, Ikhouane F, Rodellar J. The hysteresis Bouc–Wen model, a survey. Arch Comput Methods Eng 2009;16:161–88.
[19] Tounsi N, Otho A. Dynamic cutting force measuring. Int J Mach Tool Manuf 2000;40:1157–70.
[20] Guegan P, Guetari Y, Poitou A. Analyse expérimentale de la coupe orthogonale sur dispositif équipé d'une barre de Hopkinson et de caméras vidéos rapides. In: Proceedings of 17e Congrès Français de Mécanique, France; 2005 (in French).
[21] Lin C-J, Yang S-R. Precise positioning of a piezo-actuated stages using hysteresis-observer base control. Mechatronics 2006;16:417–26.
[22] Borel MO, Nicoll AR, Schläpfer HW, Schmid RK. The wear mechanisms occurring in abradable seals of gas turbines. Surf Coat Technol 1989;39/40:117–26.